Annales Geophysicae (2002) 20: 1647–1661 © European Geosciences Union 2002

Annales Geophysicae

Velocities of auroral coherent echoes at 12 and 144 MHz

A. V. Koustov[1,3], D. W. Danskin[1], M. V. Uspensky[2,4], T. Ogawa[3], P. Janhunen[2], N. Nishitani[3], S. Nozawa[3], M. Lester[5], and S. Milan[5]

[1]Institute of Space and Atmospheric Studies, University of Saskatchewan, 116 Science Place, Saskatoon, S7N 5E2 Canada
[2]Finnish Meteorological Institute, Vuorikatu 15A, P.O. Box 503, Helsinki FIN-00101, Finland
[3]Solar-Terrestrial Environment Laboratory, Nagoya University, 3–13 Honohara, Toyokawa, Aichi 442, Japan
[4]Murmansk State Technical University, Sportivnaya 13, Murmansk, 183010 Russia
[5]Department of Physics and Astronomy, University of Leicester, Leicester, LE1 7RH UK

Received: 19 November 2001 – Revised: 15 April 2002 – Accepted: 13 May 2002

Abstract. Two Doppler coherent radar systems are currently working at Hankasalmi, Finland, the STARE and CUTLASS radars operating at ∼144 MHz and ∼12 MHz, respectively. The STARE beam 3 is nearly co-located with the CUTLASS beam 5, providing an opportunity for echo velocity comparison along the same direction but at significantly different radar frequencies. In this study we consider an event when STARE radar echoes are detected at the same ranges as CUTLASS radar echoes. The observations are complemented by EISCAT measurements of the ionospheric electric field and electron density behaviour at one range of 900 km. Two separate situations are studied; for the first one, CUTLASS observed F-region echoes (including the range of the EISCAT measurements), while for the second one CUTLASS observed E-region echoes. In both cases STARE E-region measurements were available. We show that F-region CUTLASS velocities agree well with the convection component along the CUTLASS radar beam, while STARE velocities are typically smaller by a factor of 2–3. For the second case, STARE velocities are found to be either smaller or larger than CUTLASS velocities, depending on the range. Plasma physics of E-and F-region irregularities is discussed in attempt to explain the inferred relationship between various velocities. Special attention is paid to ionospheric refraction that is important for the detection of 12-MHz echoes.

Key words. Ionosphere (ionospheric irregularities; plasma waves and instabilities; auroral ionosphere)

1 Introduction

The high-latitude ionosphere always has fine structure, with irregularities being present at all heights from the bottom of the D-region to the top of the F-region (Fejer and Kelley, 1980; Tsunoda, 1988). Over the years, significant efforts have been made to understand the nature of ionospheric wave-like irregularities elongated with the Earth's magnetic flux lines. Important contributions to this area have been made through VHF radar observations of coherent echoes (Sahr and Fejer, 1996; Schlegel, 1996). VHF radars are sensitive to meter-scale irregularities in the E-region. It is well established now that these irregularities are produced by the Farley-Buneman (FB) and gradient-drift (GD) plasma instabilities, although other plasma instabilities, effective primarily at the bottom of the E-region, have been recently contemplated (e.g. Dimant and Sudan, 1995, 1997; Kagan and Kelley, 1998, 2000). Another potential source of meter-scale irregularities at the bottom of the E-region is neutral wind turbulence (Gurevitch et al., 1997). For VHF radar observations at high-latitudes, detection of coherent echoes above the E-region is practically impossible, since the radio waves reach the field-aligned irregularities at very large off-orthogonal (aspect) angles, resulting in backscatter power too low to be detected.

Over the last decade, with the introduction of a number of the Super Dual Auroral Network (SuperDARN) coherent radars (Greenwald et al., 1995), operating at HF, information on the high-latitude irregularities of decameter scale has become available. Moreover, since strong radio-wave refraction is possible at HF, even for ordinary conditions, such systems can potentially observe irregularities at nearly all heights wherever they exist. Obviously, a combination of VHF and HF radars can provide important information on irregularity properties and excitation conditions, both at different scales and at different heights.

Recently, attempts have been made to combine HF (12 MHz) and VHF (50 MHz) observations for studies of E-region high-latitude irregularities (Koustov et al., 2001; Makarevitch et al., 2001). These measurements showed differences in properties of meter and decameter irregularities. However, the conclusions of these studies are subject to the uncertainty in the amount of refraction that is experienced by radar waves at both frequencies. In this respect, more certain conclusions can be made in the case of a VHF system that has higher frequency and thus, is less sensitive to iono-

Correspondence to: A. V. Koustov
(koustov@dansas.usask.ca)

spheric refraction.

Radar measurements that are currently under way at Hankasalmi, Finland are extremely convenient for joint VHF/HF studies of auroral irregularities. Here, the HF Co-operative UK Twin Located Auroral Sounding System (CUTLASS) radar (8–20 MHz), run by the University of Leicester, UK (CUTLASS is a part of the SuperDARN network) is co-located with the VHF STARE radar ($\sim$ 144 MHz), operated by the Finnish Meteorological Institute, Helsinki. Moreover, some beams of these radar systems overlap so that a comparison of range profiles of echo characteristics can be performed without any additional assumptions regarding their azimuthal variations. In addition to these two coherent systems, the tristatic EISCAT incoherent radar (the main facility at Tromsø) can measure ionospheric plasma parameters in both E- and F-regions. In the CP-1K mode, the area of EISCAT measurements is located within one of the STARE and one of the CUTLASS radar beams.

In this study we consider nearly simultaneous observations of coherent echoes by STARE and CUTLASS along one direction with the goal to establish differences and similarities in Doppler velocity distributions and thus, give new information on the plasma physics of irregularity formation. We also perform a more detailed analysis of VHF/HF echo velocities and plasma convection at the EISCAT spot. One should say that in spite of a more or less continuous operation of the CUTLASS and STARE radars, common events with reasonable data overlap are not frequent. A requirement to have simultaneous EISCAT measurements limited dramatically the number of events suitable for studying. By searching through the common data base (with EISCAT operating in the CP-1 mode) over several years, we were able to identify only 2 events of reasonable quality, and only one of these is discussed in this study (this event exhibits more clear features).

2 Experiment setup

Figure 1 shows the experiment configuration. The broad fan-like zone is the cutlass radar field-of-view (FoV) for slant ranges between 300 and 1200 km, assuming the height of 110 km. Dashed lines indicate the ranges of 600 and 900 km from Hankasalmi. The lightly shaded area within the CUTLASS FoV is the location of the CUTLASS beam 5 (assuming the width of 5°; the actual beam width can be slightly different depending on radar frequency), and the darker shading is the STARE beam 3. The STARE beam is slightly shifted to the west of the CUTLASS beam's center and has the beam width of 3.2°. For the analysis, these beams were selected since they reasonably overlap and there is also an area where joint measurements with the EISCAT incoherent scatter radar are possible. The solid circle in Fig. 1 represents the location of EISCAT area of measurements (at 300 km) in CP-1K mode. Note that the real diameter of the EISCAT collecting area is $\sim$ 1 km in the E-layer and $\sim$ 2.5 km in the F-layer, meaning that the EISCAT spatial resolution is at least one order of magnitude finer than the coherent radars. The distance

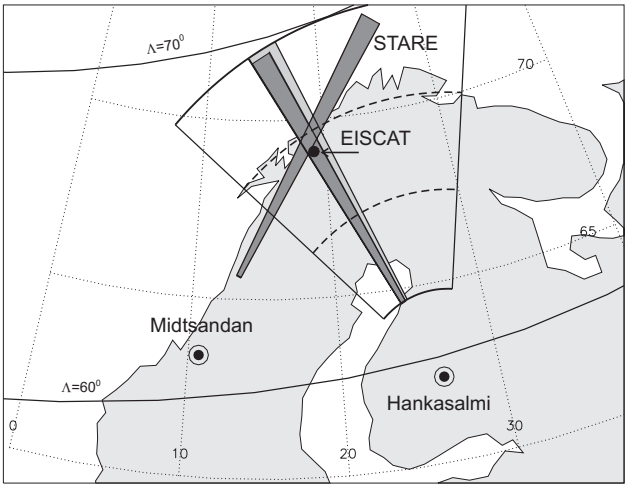

Fig. 1. Field-of-view of the Hankasalmi CUTLASS HF radar for ranges between 300 and 1200 km at the height of 110 km. Dashed lines are slant ranges of 600 and 900 km. The lightly shaded sector is the location of the CUTLASS beam 5. The darker beam-like sectors are the location of the Finland STARE radar beam 3 and the Norway STARE radar beam 4. The solid dot denotes the area where ionospheric parameters were monitored by the EISCAT incoherent scatter radar. Also shown are PACE lines of equal magnetic latitudes $\Lambda = 60°$ and $\Lambda = 70°$.

from Hankasalmi to the EISCAT collecting area is around 900 km (for the height of $\sim$ 300 km). We also show the location of beam 4 of the second STARE radar (140 MHz) operated at Midtsandan (Norway) by the Max-Plank Institute, Lindau. The intersection of the chosen STARE radar beams is very close to the area of the EISCAT measurements. The distance from Midtsandan to the EISCAT spot is about 750 km. In Fig. 1 the PACE magnetic latitudes of 60° and 70° are presented for the reader's convenience.

We focus in this study on the event of 12 February 1999, 10:00–18:00 UT. During this period, all radars were in their standard modes. The HF CUTLASS radar (12.4 MHz) was operated in the fast common mode, which completes one full sweep over the FoV in one minute. The radar scanned through 16 beam positions, starting a scan at the beginning of each minute with a dwell time in each beam position of about 3 s. Echo power, Doppler velocity and spectral width were determined in 45-km range bins from 180 km to ranges well beyond the E-region radio horizon of 1200 km.

The STARE VHF radars (144/140 MHz) had a 15-km range resolution, starting at 495 km and a 20 s integration time. The standard single-to-double pulse pattern was used (Greenwald et al., 1978) to resolve the power and Doppler velocity profiles.

The EISCAT radar was in CP-1K mode with the transmitter beam at Tromsø being oriented along the local magnetic flux line, with the receiver beams at Kiruna and Sodankyla being oriented to a common volume. All three beams were intersecting at the height of 250 km to perform tri-static measurements of the ionospheric electric field. In

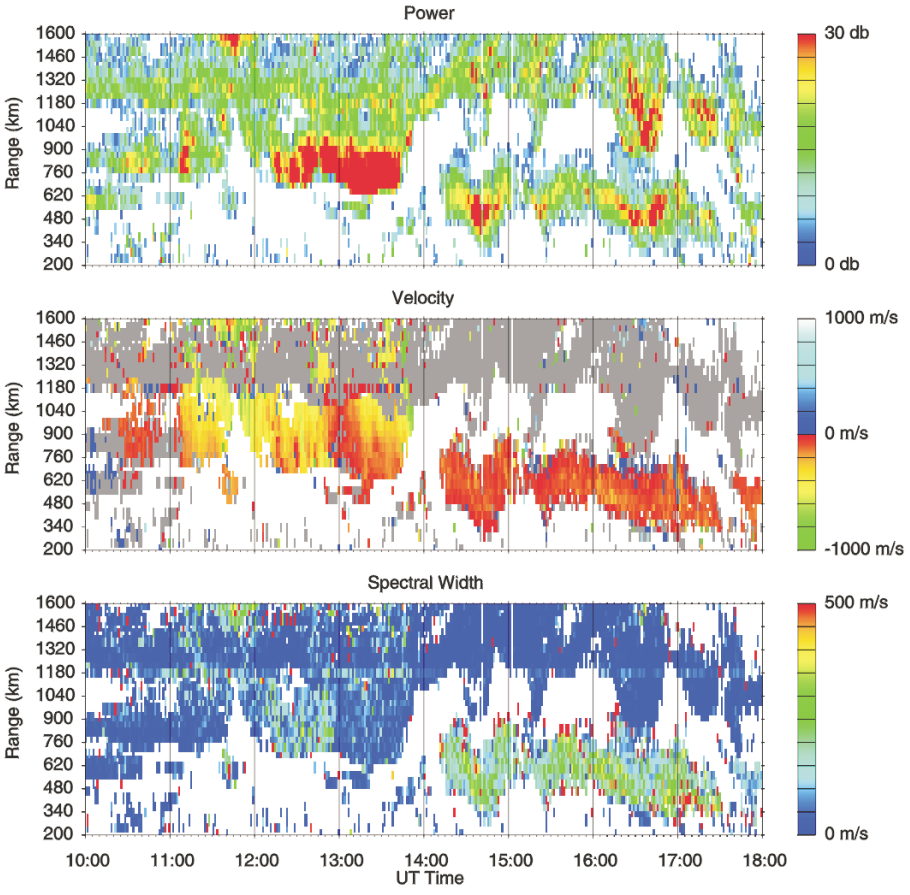

Fig. 2. Plots of CUTLASS HF echo power, Doppler velocity and spectral width versus time in beam 5 for the event of 12 February 1999, 10:00–18:00 UT.

addition, measurements of the electron density were performed from ∼90 km to ∼300 km along the Tromsø beam. The altitude resolution of density measurements was 3.1 km below ∼180 km and 22 km above ∼180 km. We used 2-min averaged data to ensure that the timing was as close as possible to the integration time of coherent radars. Since the 3 radar systems did not coordinate the timing of the measurements, there were some differences in time between data records, but these differences were less than 1 min.

3 Event overview

The twelfth of February 1999 was a moderately disturbed day (Coffey, 1999) with low local magnetic activity over Scandinavia, seen by the IMAGE magnetometer network between 10:00 UT and 13:00 UT (magnetic perturbations <+100 nT) and some activity afterwards. A smooth enhancement of an eastward electrojet (perturbations <+250 nT) was observed between 14:30 UT and 15:00 UT followed by another intensification between 15:00 and 15:30 UT. A third activation after 16:00 UT was followed by 2 short-lived intrusions of a westward electrojet (magnetic perturbations stronger than −250 nT) at latitudes poleward of Tromsø.

CUTLASS echoes were detected during almost the whole period under discussion, but in two bands of ranges that were quite different, Fig. 2. Prior to 14:00 UT, echoes were located at large ranges of 700–1100 km. Interferometer measurements showed that these were F-region echoes. By employing ray tracing, Danskin et al. (2002) showed that for the period under consideration, one would expect the presence of F-region echoes at 800–1200 km and E-region echoes at shorter ranges (their Fig. 7). There were seen only some short-lived echoes at short ranges (Fig. 2). One of the possible reasons for the absence of these short-range echoes is a strong electric field decrease with latitude; we demonstrate the effect later by showing that the CULTASS velocity decreases at shorter ranges.

After 14:00 UT, echoes were continuously seen at much shorter ranges, typically 400–700 km, with some slow displacements of the echo band in the north-south direction. According to the interferometer measurements, these were E-region echoes. Generally, one can expect F-region echoes at farther ranges at these times, since according to EISCAT, the electric field was quite significant at that part of the ionosphere and one would expect the decameter irregularities being present at the F-region heights. However, no F-region echoes were detected. By employing ray tracing, we show later (see Fig. 13 in Discussion) that due to a quite dense E-region at these times, the F-region decameter irregularities were simply not accessible to HF radio waves. During the periods of F- and E-region HF echo observations, measured HF

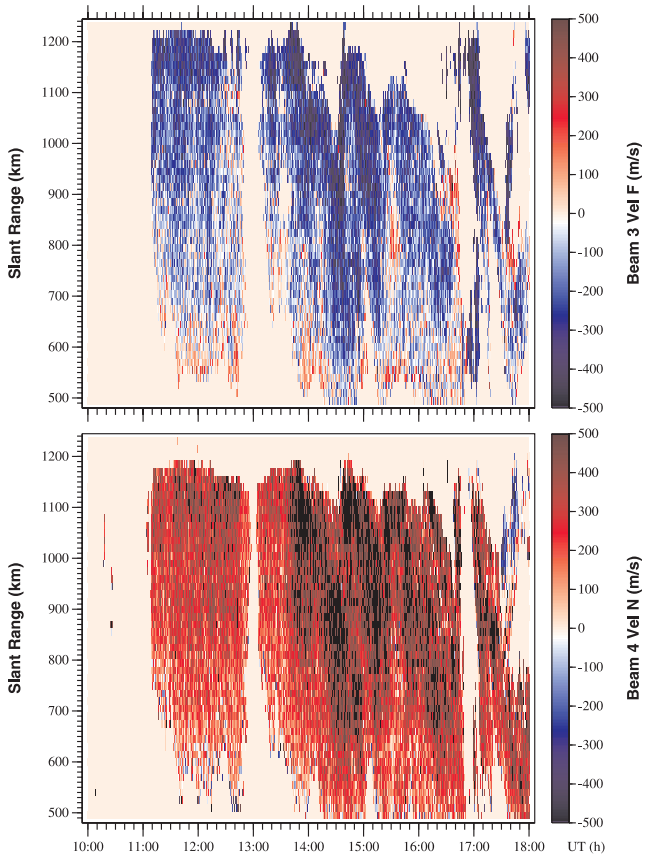

Fig. 3. Plots of STARE VHF echo Doppler velocity versus time in beam 3 for the Finland radar and beam 4 for the Norway radar for the event of 12 February 1999, 10:00–18:00 UT.

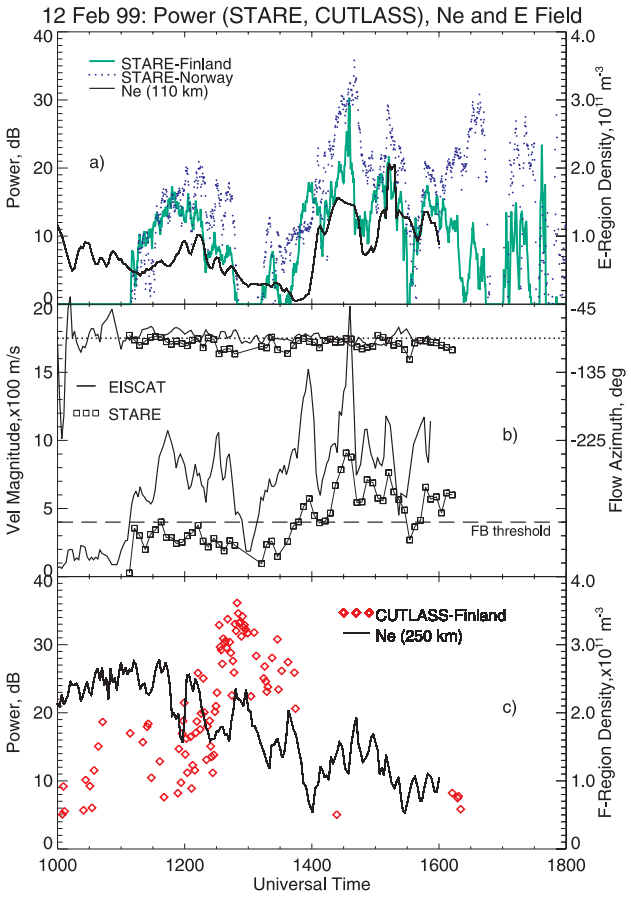

Fig. 4. **(a)** Temporal variations of Finland STARE (green dots) and Norway STARE (blue dots) echo power in bins 27 and 17, respectively. Power of the Norway radar was scaled down by 2.4 dB to take into account the shorter distance to the scattering volume. Solid line shows the electron density at 110 km according to EISCAT measurements. **(b)** Plasma convection velocity magnitude and azimuth according to EISCAT tri-static measurements at 250 km (solid line) and STARE convection magnitude/direction estimates (squares). **(c)** The Hankasalmi CUTLASS echo power (red diamonds) versus time and the electron density at 250 km according to EISCAT measurements.

velocities were quite different and large, up to 200–600 m/s in the first case and low, 100–200 m/s, in the second case.

STARE registered echoes between about 11:00 UT and 18:00 UT in a broad band of ranges, starting from about 500–600 km all the way to the radio horizon of 1200 km, Fig. 3. STARE velocities for both radars were quite variable, with lower velocities at near distances and larger velocities at far distances. This trend was perhaps partially associated with a general decrease in the electric field with latitude.

A more detail presentation of the data is given in Figs. 4a–c and 5a–c. In Fig. 4a we show the power of Hankasalmi and Midtsandan echoes at ranges close to the EISCAT range (bin 27 for Hankasalmi and bin 17 for Midtsandan) for the whole event. The Norway echoes are obviously stronger. One observes quite synchronous temporal variations of the power. In Fig. 4a we also show the electron density at the height of 110 km, roughly at the center of the electrojet layer. According to the EISCAT measurements, the density profiles most of the time exhibited a broad maximum near 110–120 km. One notices the correlation between the STARE echo power increases (for both radars) and the electron density enhancements, a well-known effect at VHF (Starkov et al., 1983; Williams et al., 1999).

Figure 4b shows the electron drift (opposite to plasma convection) magnitude and direction (solid line), as observed by EISCAT (the data were smoothed with a 5-point sliding window). The direction is measured from geographic north, positive to the east. The electron flow is quite fast, in excess of 400 m/s for the majority of the time (see horizontal dashed line). This means that the threshold condition for the FB plasma instability excitation is met most of the time. The flow is predominantly westward (eastward electrojet). One can clearly see a correlation between the decrease in STARE power in Fig. 4a (no echoes before 11:00 UT and around 13:00 UT, low power near 15:30 UT) and the decrease in the electric field. We also show in Fig. 4b the azimuth and magnitude of the electron flow, as derived from the standard

STARE merging procedure (squares). One can see a reasonable agreement in the STARE and EISCAT azimuths and a significant STARE underestimation of the flow magnitude, in agreement with earlier results by Nielsen and Schlegel (1985).

In Fig. 4c we show electron density at 250 km (EISCAT). In the F-region, density profiles were fairly flat between heights of 220 and 270 km (though sometimes with quite a variability from one height to the next one), exhibiting a broad maximum around 250 km. We also present in this diagram the CUTLASS echo power as measured near the EISCAT spot, the red diamonds. One can see that the HF echoes are received for F-region densities around 2.0×10^{11} m^{-3}. Such electron density is sufficient to provide the radio-wave orthogonality at the height of 180–230 km (Danskin et al., 2002) thus, confirming that the CUTLASS echoes between 12:00 UT and 14:00 UT were indeed coming from the F-region heights.

An overview of the velocity measurements of all radars is presented in Figs. 5a–c. In Fig. 5a we show the EISCAT velocity component (solid line) projected along the direction of the STARE-Finland radar beam 3 (as expected under the assumption that the VHF Doppler velocity is a cosine component of the total drift). We superimpose the Doppler velocity (green points) measured by the STARE-Finland radar in beam 3, bin 27. Since the spread of points is significant, we indicate the smoothed temporal variation of the Doppler velocity by a solid green line. One can see some general agreement in temporal variations of the velocities, although the STARE velocity is typically smaller than the EISCAT velocity by a factor of 2–3. Also shown in Fig. 5a is the ion-acoustic speed (we assigned a negative sign for the convenience of presentation) at $\sim$111 km, according to EISCAT measurements. We assumed that both electrons and ions are isothermal, and the ion mass is 31 amu. One can see that most of the time the EISCAT velocity component along the Finland radar beam 3 (and the Finland radar Doppler velocity as well) was below the ion-acoustic speed, meaning that the Finland STARE radar was observing electrojet irregularities outside the FB instability cone.

Figure 5b shows similar data for the EISCAT velocity along the STARE-Norway radar beam 4, the STARE-Norway Doppler velocity in bin 17 (plotted with the opposite sign for the convenience of presentation) and the ion-acoustic speed at $\sim$111 km (we also assigned a negative sign for it). Here the STARE/EISCAT agreement is slightly better, though the STARE velocity is still almost always smaller than the EISCAT velocity. Both the EISCAT velocity component along the Norway beam 4 and the Norway Doppler velocity have smaller magnitudes than the ion-acoustic speed most of the time, meaning that this radar was also observing irregularities outside the FB instability cone.

Figure 5c compares the EISCAT velocity component along the CUTLASS beam 5 and the CUTLASS Doppler velocity at $\sim$900 km. Contrary to the STARE case, the agreement is much better, though there is a tendency for the CUTLASS velocity to be slightly smaller. One can notice a lack

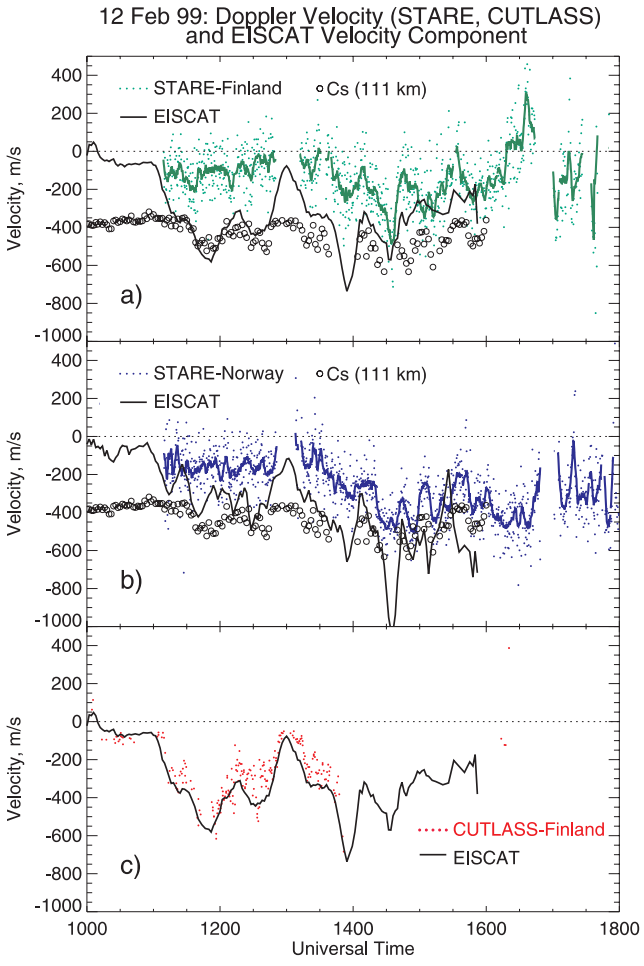

Fig. 5. **(a)** Finland STARE (green dots) beam 3 Doppler velocity in bin 27 versus time and the EISCAT convection component (solid line) along beam 3. The solid green line represents smoothed behaviour of the STARE velocity. **(b)** Norway STARE (blue dots) beam 4 Doppler velocity in bin 17 and the EISCAT convection component (solid line) along beam 4 versus time. The blue solid line represents smoothed behaviour of the STARE velocity. **(c)** Hankasalmi CUTLASS beam 5 Doppler velocity (red dots) in bin 16 and the EISCAT convection component (solid line) along this beam versus time.

of CUTLASS echoes after 14:00 UT; at this time the echo band was located at shorter ranges, see Fig. 2.

4 Aspect angle conditions for coherent radars

We show in this study that the aspect angle conditions of measurements are important for understanding obtained results. For this reason, we consider them in detail in this section. Figure 6a shows the aspect angle (at various heights) versus slant range for both HF and VHF Hankasalmi radars and the azimuth of $-20.8°$ (beam 3 of STARE). A simple geometric-optics approach was employed, similar to Uspensky et al. (1994). The uniform electron density of 5×10^{10} m^{-3} has been adopted, though the STARE aspect angles

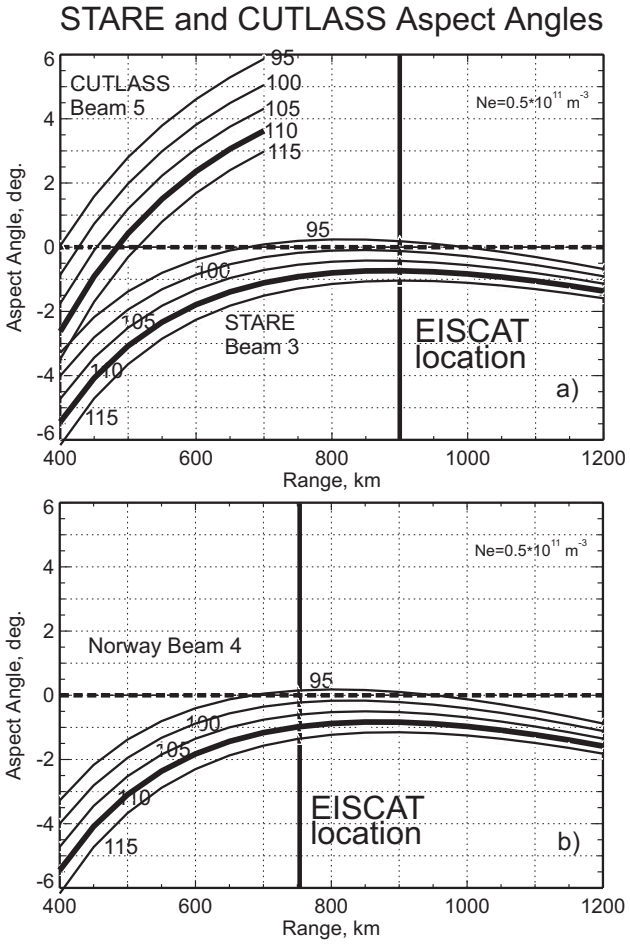

Fig. 6. Aspect angles versus slant range at various heights for **(a)** Norway STARE radar beam 4, **(b)** Finland STARE radar beam 3 and Hankasalmi CUTLASS radar beam 5. An electron density of 5×10^{11} m^{-3} was assumed.

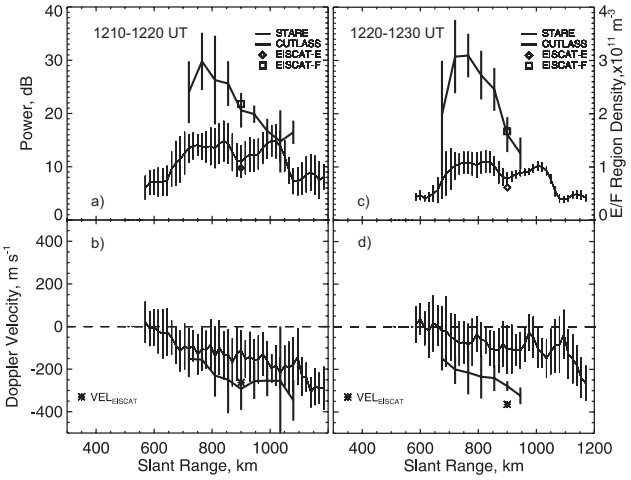

Fig. 7. Averaged slant range profiles of echo power **(a, c)** and Doppler velocity **(b, d)** for two 10-min periods of joint STARE/CUTLASS observations when CUTLASS observed F-region echoes and STARE observed E-region echoes. An asterisk (in b, d) shows EISCAT convection component along the direction of observations at the range of 900 km. Square and open diamond (in a, c) show the average electron density at the heights of 250 and 110 km, respectively. Scale for the densities is shown to the right of panel (c).

do not change much for electron densities typically observed in the auroral ionosphere.

One can see that the STARE aspect angles are negative at all slant ranges. Negative aspect angles mean that additional refraction of radio waves is required to meet magnetic flux lines orthogonally. At the height of 110 km, the aspect angles are of the order of $-0.8°$ at ranges 800–1000 km and they go down fairly quickly at shorter ranges. The STARE aspect angles are better at lower heights. Calculations show that in the F-region (250 km), the aspect angles range from $-25°$ at short distances, to $-8°$ near the radio horizon. The STARE-Norway aspect angles, presented in Fig. 6b, show variations similar to the ones by the STARE-Finland radar, with aspect angles at the EISCAT spot of about $-1°$ at the height of 110 km.

The CUTLASS aspect angles exhibit a more dramatic change with range. They are strongly negative at distances of less than 400–500 km and positive at distances beyond $\sim$500–600 km. The location of the point with zero aspect angle (at every height) is very sensitive to the choice of the electron density; this point is located farther (closer) away (towards) from the radar with density decrease (increase). A more thorough, full ray-tracing analysis for the most recent AACGM magnetic field model shows that the range of near-zero aspect angles at HF is in between 450 and 550 km, depending on height. The fact that the aspect angles presented in Fig. 6a are not extremely precise is not so important for this study, because there is much more serious uncertainty in the electron density profile and its latitudinal variation. In the F-region (250 km), the CUTLASS aspect angles are several degrees better than at 140 MHz, but still quite large for chosen electron density.

An important conclusion of these calculations is that the aspect angles for both STARE radars are almost nowhere perfect. The aspect conditions quickly deteriorate at distances of less than 600–700 km, whereas near perfect aspect conditions for the CUTLASS radar can be met in a broad band of ranges, from 400 km to 1200 km, depending on the electron density in the E- and F-regions.

5 Details of the velocity relationship

One of the goals in this study is to compare HF and VHF velocities. We do this in two different ways. First, we consider averaged slant range profiles of the power and velocity with averaging over 10-min intervals (we consider periods during which a 1-min comparison shows reasonable agreement). Our second approach is to compare VHF and HF velocity data at similar ranges and for the time separation of less than 1 min. We explore then the relationship of HF/VHF

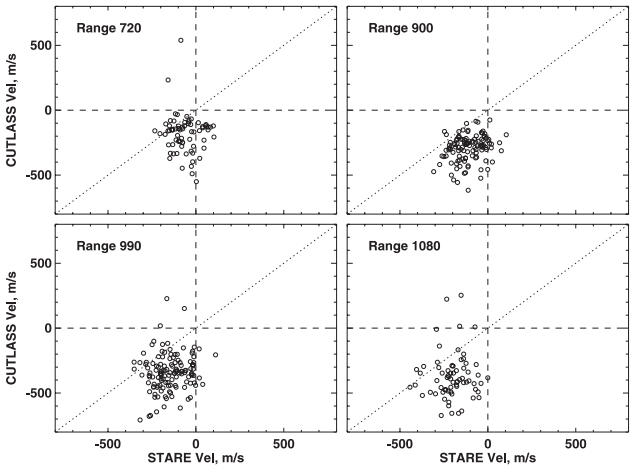

Fig. 8. Scatter plot of Hankasalmi CUTLASS velocity versus Finland STARE velocity at several slant ranges for the period of 11:00–14:00 UT when CUTLASS (STARE) radar observed echoes from the F- (E)-region.

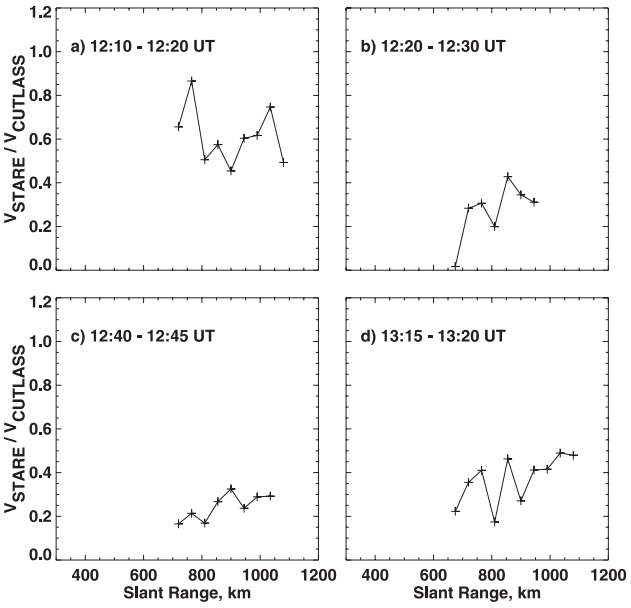

Fig. 9. Range profiles of the velocity ratio $R = V_{\mathrm{STARE}}/V_{\mathrm{CUTLASS}}$ for several periods of measurements.

velocities and plasma convection monitored by EISCAT at a range of 900 km.

5.1 F/E comparison

The first half of the considered period corresponded to the case when the CUTLASS radar observed F-region scatter while both STARE radars, as always, observed E-region scatter. We call such situation the F/E case.

5.1.1 Range profiles

Typical examples of power and velocity range distributions for two 10-min intervals during this period are presented in Figs. 7a–d. Here the data are averaged for each range of observations; thin and thick lines show STARE (Finland) and CUTLASS measurements, respectively. Vertical bars indicate the standard deviations of the parameters at each range. No range corrections were applied for the power of both radars. Ranges with less than 5 points for CUTLASS and 13 points for STARE (less than half of the potentially possible measurements) are not considered. Typically for each range, there were 6–8 points for CUTLASS and more than 20 points for STARE. In Figs. 7a and c we also show at 900 km the averaged densities as measured by EISCAT at 110 km (open diamond) and 250 km (square). In Figs. 7b and d we show by asterisk the averaged velocity component at 900 km as measured by EISCAT.

One can see that the range coverage for CUTLASS is smaller than for STARE. In terms of power, CUTLASS shows fairly clear maxima at ranges ~ 750 km, while STARE shows much more uniform distributions with steady power decreases at short distances. This decrease is consistent with the deterioration of aspect conditions and perhaps some electric field decrease at short ranges. Also, the CUTLASS power profile in Fig. 7c is shifted slightly towards larger ranges than in Fig. 7a, most likely due to a decrease in the F-region electron density. STARE and CUTLASS velocities are different at all ranges, from 700 to 1100 km, with the velocity ratio of the order of 0.5. At the point of EISCAT measurements, the CUTLASS velocity is close to the EISCAT velocity component on Fig. 7b and slightly smaller on Fig. 7d, consistent with the data presented in Fig. 5c. Magnitudes of HF velocity are smaller at shorter ranges. This happens, most likely, due to an electric field decrease at lower latitudes, a commonly seen effect in the afternoon sector (Rich and Hairston, 1994).

In Fig. 8 we compare STARE and CUTLASS velocities for measurements with time separation of less than one minute. We use STARE data averaged over three successive 15-km bins (to match 45-km bins of CUTLASS). One can see that the STARE velocities are systematically smaller than the CUTLASS velocities at all ranges, including the range of the EISCAT measurements.

To give more a quantitative assessment of the VHF velocity with respect to the HF velocity and thus, with respect to the $\boldsymbol{E} \times \boldsymbol{B}$ (convection) component along the HF beam, we consider range profiles of the ratio $R = V_{\mathrm{STARE}}/V_{\mathrm{CUTLASS}}$. We have to keep in mind here that the CUTLASS Doppler velocities agreed well with the EISCAT convection measurements at one point (for the range of 900 km, Fig. 5c), and thus, one can treat the CUTLASS velocity range profile as the range profile of the convection component. Since the aspect angles of STARE measurements are progressively larger at shorter ranges, the expectation is that R should be smaller at shorter ranges. In Fig. 9 we present several range profiles for the ratio R, including two profiles for the data shown in Fig. 7. Three profiles out of four demonstrate the expected effect. We should note that such a tendency was not always

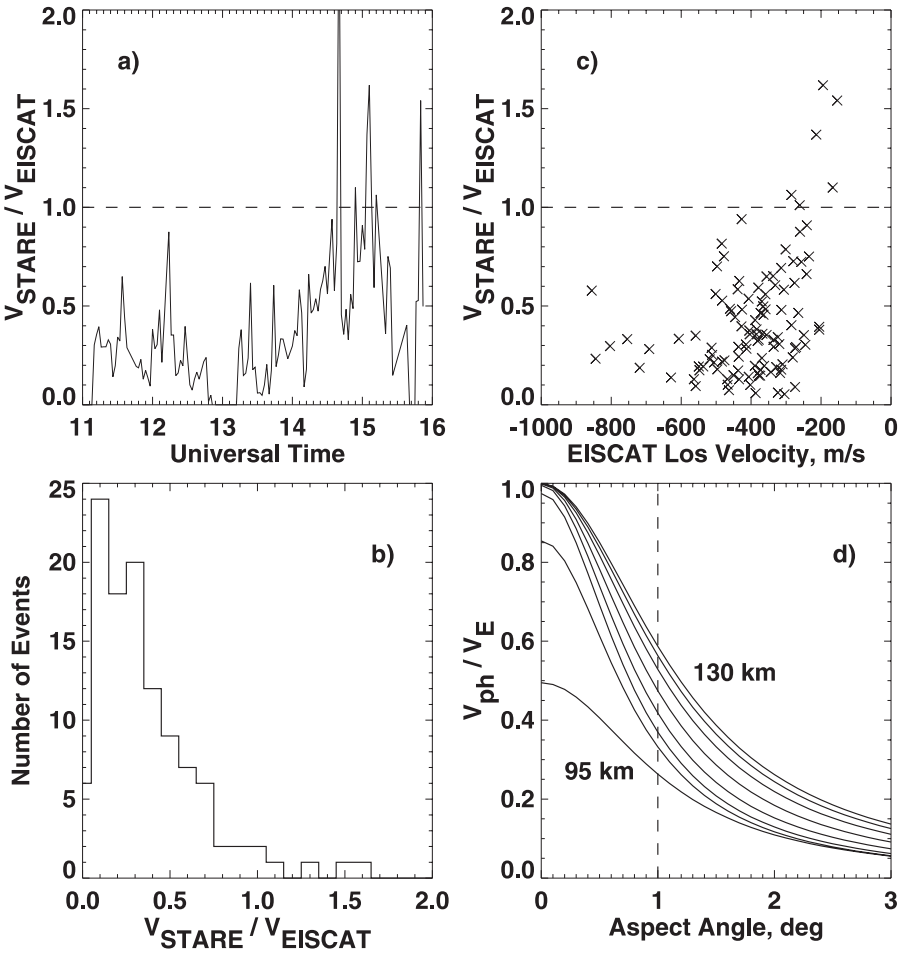

Fig. 10. Data on the observed STARE Finland velocities and linear theory expectations. **(a)** Ratio of the Finland Doppler velocity to the EISCAT convection component $R_1 = V_{\mathrm{STARE}}/V_{\mathrm{EISCAT}}$ for the whole period of observations at the EISCAT spot. **(b)** Statistics of R_1 values. **(c)** Ratio R_1 as a function of the convection component magnitude. **(d)** Ratio of the irregularity phase velocity (according to the linear fluid theory of electrojet irregularities) to the convection component as a function of the aspect angle. Curves are given for heights 95–130 km with 5-km step.

clear due to a significant data spread for both radar systems. Obviously, a statistical study of this effect is required, and this work is currently under way for the events with more stable coherent radar data.

5.1.2 Comparison at the EISCAT spot

VHF measurements at the EISCAT spot allow us to assess these velocities with respect to the $\boldsymbol{E} \times \boldsymbol{B}$ velocity component measured by the EISCAT radar (V_{EISCAT}). We show in Fig. 10a the ratio $R_1 = V_{\mathrm{STARE}}/V_{\mathrm{EISCAT}}$ for the whole period under study. Here we used the data of Fig. 5a that we averaged over 2-min intervals. Figure 10b gives the distribution of R_1 values. The more frequently occurring R_1 is ~ 0.2, though all values between 0.1 and 1.0 are possible. Figure 10c shows R_1 versus V_{EISCAT}. Though the data spread is significant, one can recognize that R_1 tends to decrease with the velocity (electric field), something one would expect from the kinetic theory of the FB instability (Schlegel, 1983). Figure 10d shows expected values for the ratio of the irregularity phase velocity and the $\boldsymbol{E} \times \boldsymbol{B}$ component (V_{ph}/V_{E}) for various aspect angles and at different ionospheric heights, according to the linear theory of the FB and GD instabilities (95–130 km, the step in height is 5 km). The standard formula (Fejer and Kelley, 1980) was used with the ion term contribution being neglected, similar to Kustov et al. (1990) and Uspensky et al. (1994). The electron-neutral and ion-neutral collision frequencies used in the calculations were computed similarly to Schlegel (1983) by selecting the MSIS-90 atmospheric model for the latitude, longitude and period under study. One can see from Fig. 10c that at the aspect angle of 1° the irregularity phase velocity can be smaller than the convection component by a factor of 2–3, depending on the height in the ionosphere, in rough agreement with the observations.

5.2 E/E comparison, range profiles

For the second period between 14:00 and 18:00 UT both STARE and CUTLASS echoes were received from the E-region, and we explore these data in this section. Figures 11a–d show data in the same format as in the F/E case of Figs. 7a–d. Again, the STARE range coverage is more significant than the CUTLASS coverage. One can see that this time the CUTLASS echo regions are shifted more towards the radar than the STARE echo regions, in agreement with enhanced E-region density in this case, when compared with Fig. 4a. Interestingly enough, the maxima of the STARE

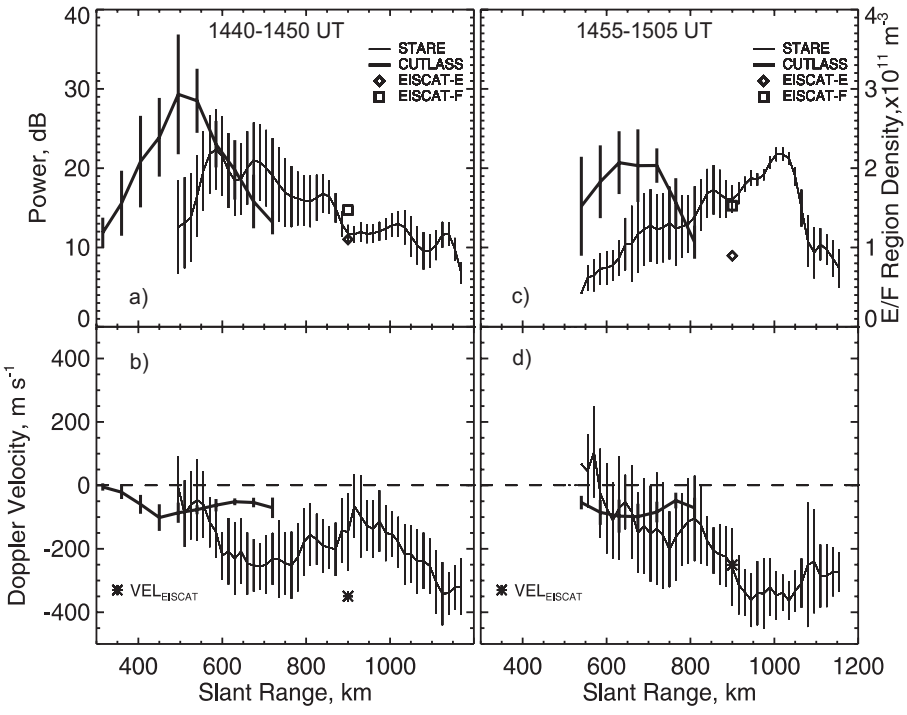

Fig. 11. Similar to Fig. 7 except for periods when both CUTLASS and STARE observed E-region echoes.

power profiles are shifted (e.g. in Fig. 11a) to shorter ranges, where the geometric aspect angle conditions are not the best. This may indicate that a localized region with enhanced density was set up at these ranges. One can also notice a shift in the HF echo power maximum in Fig. 11a to slightly larger ranges in Fig. 11c, which is consistent with the decrease in E-region electron density.

The STARE velocity profiles are very much similar to the previous case (Figs. 7b and d) in that the velocity decreases as the range decreases. The velocity magnitudes are small at short ranges, less than 100 m/s, but they exceed 200 m/s at at farther ranges of $\sim$700–800 km. At the range of the EISCAT measurements, the STARE velocity is smaller than the EISCAT convection component in the case of Fig. 11b, and velocities are close to each other in the case of Fig. 11d. Contrary to the more or less monotonic decrease in STARE velocities at shorter ranges, CUTLASS velocities exhibit a clear maximum in Figs. 11b and d, and this maximum is located near the ranges of the CUTLASS power maximum. The CUTLASS velocities are roughly the same as the STARE velocities at the range of the CUTLASS power maxima. In Fig. 11d, the CUTLASS velocities are larger than the STARE velocities at several short ranges and smaller at large ranges.

Scatter plots of CUTLASS versus STARE velocities for some slant ranges are given in Fig. 12. One can see that points cluster around the bisector of perfect agreement and departures both ways are possible. However, for most ranges (exceptions are the shortest ranges, e.g. 495 km) the predominant trend is for CUTLASS velocity to be smaller than the STARE velocity.

6 Discussion

In this study we compared velocity data from CUTLASS (12.4 MHz) and STARE (144 MHz) coherent radar systems. The data were gathered in the early evening sector, during a period of moderate magnetic activity and at large flow angles. In addition, we were able to check how the observed velocities agree with the plasma convection at one slant range where the EISCAT data were available.

6.1 Is STARE velocity a cosine component of convection?

Two distinctly different situations were encountered. First, we considered the case for which the HF radar was observing echoes from the F-region, while the VHF radar was monitoring backscatter from the E-region. For this situation, we had simultaneous EISCAT convection and electron density data, though at only one range of 900 km. Observed HF Doppler velocities were found to match the EISCAT plasma convection component along the HF radar beam reasonably well. Thus, we once again demonstrated the good overall performance of the HF radars for plasma convection measurements reported earlier (e.g. Davies et al., 1999). This result allowed us to assume that the observed CUTLASS velocity range profiles (for F-region echoes) corresponded to the range profiles of the convection component along this beam.

The central issue for the F/E comparison was by how much the VHF velocity differed from the "cosine" convection component. For observations along the electrojet (inside the FB instability cone), this question has been studied in a number of papers (e.g. Providakes et al., 1988; Haldoupis and Schlegel, 1990). There has not been so much focus on ob-

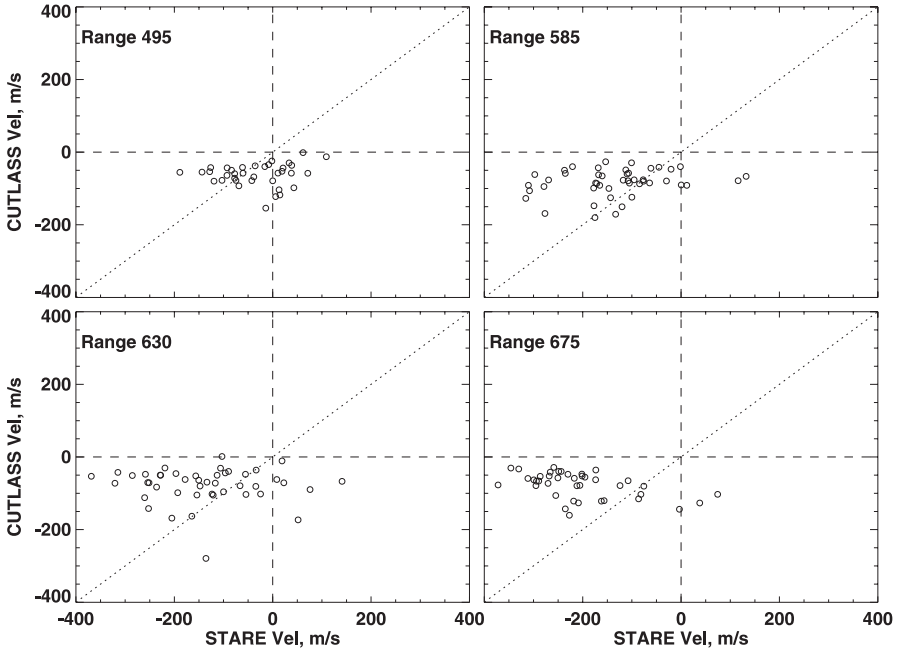

Fig. 12. Scatter plot of Hankasalmi CUTLASS velocity versus Finland velocity at several slant ranges for the period of 14:00–18:00 UT when both CUTLASS and STARE radars observed echoes from the E-region.

servations outside the FB instability cone. Up to now, the prevailing notion is that there is not much difference between these two velocities (Nielsen and Schlegel, 1985; Reinleitner and Nielsen, 1985; Nielsen et al., 2002), although Robinson (1993) seriously questioned the validity of the "cosine rule" for the STARE measurements. One should note that recent velocity statistics by Nielsen et al. (2002) shows significant departures from the cosine law for some individual points (see their Fig. 4, flow angle of +10°), though the authors still make a conclusion that the VHF velocity varies according to the cosine law.

We employed two approaches to the problem, by comparing VHF and HF velocities at various ranges and by comparing VHF velocities with the EISCAT convection data at one range. In both cases we found that VHF velocities were considerably smaller than the convection component. Differences by a factor of ~ 3 were observed, especially at short ranges of ~ 700 km. One might expect this result on the basis of earlier studies (e.g. Kustov and Haldoupis, 1992; Kohl et al., 1992). We found that the velocity differences in our case were considerably larger than in Kustov and Haldoupis (1992) and comparable to the ones reported by Kohl et al. (1992) for several short periods of a rocket flight in the ROSE campaign.

One should mention that the F/E velocity comparison (for various ranges) has been made by neglecting the fact that HF and VHF scatter was actually coming from different heights. This means that there are some errors in the relative positioning of the STARE and CUTLASS echoes with range in Figs. 7a–d. The errors are of the order of one radar bin (André et al., 1996), i.e. 45 km. Inspection of range profiles given in Figs. 7a–d shows that this uncertainly does not change the above conclusion; the STARE velocities are smaller than the EISCAT plasma convection component in all close radar bins. To explore a potential impact of this effect on the data presented in Fig. 8, we compared VHF and HF velocities by considering HF data at one range bin farther than VHF data. For this comparison (appropriate diagrams are not shown here) again VHF velocities are smaller than HF velocities.

The reasons for the stronger VHF velocity depression effect in our case are not clear. One possibility is that, for our event, the double-pulse technique used in STARE measurements was not adequately describing the phase velocity of electrojet irregularities. Schlegel and Thomas (1988) reported on occasional significant differences between double-pulse and full spectrum methods of velocity determination. More study is needed on this issue.

Potential reasons for generally smaller VHF velocity as compared to the $\boldsymbol{E} \times \boldsymbol{B}$ velocity component outside the FB instability cone was discussed by Kustov et al. (1990), Kustov and Haldoupis (1992) and Kohl et al. (1992). The first two papers proceeded from the idea that the auroral radar signal is collected from various electrojet heights, and at every height the irregularity phase velocity has a reduced value determined by the aspect angle of backscatter. The aspect angle variation for the irregularity velocity was taken into account by involving the linear fluid theory of the FB and GD instabilities. We illustrated the range of the expected effect in Fig. 10d and found it to be comparable with the measurements. One should mention that kinetic effects (Schlegel, 1983) would further decrease the values of the velocity ratio R_1 and thus, provide even better agreement between the theory and measurements. For this reason, we believe that in our event the VHF velocity decrease (relative to the EISCAT plasma convection component) for the directions outside the FB instability cone was associated with non-zero aspect angles ($>0.5°$) of the STARE measurements.

Kohl et al. (1992) attempted to explain small STARE velocities outside the FB instability cone by involving the neutral wind that modifies the irregularity phase velocity, as predicted by the linear theory of the FB and GD instabilities. However, the required wind speeds were found to be several hundred meters per second, i.e. well above the typically measured ones so that this explanation needed further examination. For our event, between 12:00 UT and 14:00 UT, MF radar measurements at Tromsø (C. Meek, personal communication) showed wind drifts below ~ 80 m/s and were quite variable in time so that application of this idea to the STARE data does not look promising.

One should mention that our conclusion on the agreement between the linear theory and measurements is in some contradiction with an earlier study by Nielsen (1986), who reported a much slower rate of velocity decrease with the aspect angle. However, one should bear in mind that Nielsen (1986) considered observations primarily along the electrojet, where plasma turbulence might play a strong role in setting up enhanced electron collisions. Ogawa et al. (1982) reported a slower rate of velocity decrease not only along the flow, but at large flow angles as well, though these authors related the latter effect to the latitudinal variations of the background electric field. Kustov et al. (1994) considered observations at large flow angles, but at aspect angles of several degrees, and also found slower rates of decrease.

An alternative explanation of the VHF velocities outside the FB instability cone that were too small is the violation of the cosine rule for the irregularity phase velocity (i.e. one might question whether the $\cos\theta$ term in the linear theory formula is applicable to STARE observations). To date, there are not much data in the literature that would support this notion. In the past, Reinleitner and Nielsen (1985), Nielsen and Schlegel (1985) and Nielsen et al. (2002) reported on the reasonable performance of the cosine rule for the STARE drift velocity directions, while Kustov et al. (1997) drew a similar conclusion for the Canadian observations at very large aspect angles. We showed that for our event (Fig. 4b) the STARE convection azimuth (inferred through the merging of the Finland and Norway velocities by the standard "stereoscopic" technique (Greenwald et al., 1978; Nielsen, 1989)) agrees well with the EISCAT observations. Though this result is expected on the basis of previous observations mentioned earlier (e.g. Nielsen and Schlegel, 1985), in our case it is still a surprise since a much stronger than usual velocity decrease with respect to the plasma convection was observed by the individual STARE radars. A reasonable agreement between the total STARE irregularity drift velocity directions and the EISCAT measurements in our event perhaps indicates that VHF velocity is proportional to the cosine of the flow angle and the observed small velocities are related to other factors, most likely to the aspect angle effects, as we explained above.

If one interprets smaller VHF velocities as the aspect angle effect, then our measurements indicate that the VHF velocity decrease with the aspect angle for irregularities propagating outside the FB instability cone is significant for quite a range of aspect angles, since decreased STARE velocities were seen at all ranges along beam 3. This means that the convection estimates by the standard merging technique and by the IAA technique of Nielsen and Schlegel (1985) (this method also assumes that Doppler velocity outside the FB cone is simply a cosine component of the flow angle) should deteriorate as one considers measurements at the equatorward and westward portions of the STARE field-of-view, where the aspect angles can be as large as $-2°$.

6.2 Why are the STARE and CUTLASS E-region velocity profiles so different?

The second case in our event was when both VHF and HF echoes were received from the E-region. In this case, the HF echoes occurred only at short ranges, where, unfortunately, no EISCAT convection measurements were available. For the E/E comparison, results were quite complicated. The HF echoes were typically observed at shorter distances, by as much as 150–200 km, and at some moments, the HF and VHF echoes were spatially located at ranges that were so different that comparison of their parameters was impossible. One unfortunate situation was when the electron density (according to the EISCAT measurements) was enhanced, the HF echo band was centered at distances of 500 km or less, where no STARE measurements were carried out (first range is 495 km). The STARE range profiles were not as sensitive to density changes. Such a contrast between the VHF and HF response to these electron density variations is expected (Uspensky et al., 1994).

For the cases with reasonable spatial overlap of STARE and CUTLASS echo bands, we found that generally the velocity relationship depended on the relative position of the HF and VHF echo power maxima so that the VHF and HF velocities can either be comparable or quite different. At shorter distances the VHF velocity was usually smaller than the HF velocity, while at larger distances it was the other way around, where the HF velocity was smaller than the VHF velocity (here and below when we say velocity we mean the velocity magnitude). It is then not a surprise that when HF and VHF velocities were compared for the same ranges and time, Fig. 12, there were point deviations both ways; the VHF velocity was larger than the HF velocity for some measurements and less than the HF for other measurements. One should note that Davies et al. (1999) reported that the CUTLASS velocities were typically smaller than the $\boldsymbol{E} \times \boldsymbol{B}$ component along the HF radar beam (their Fig. 5). This result agrees with our finding. Koustov et al. (2001) and Makarevitch et al. (2001) also reported smaller HF velocities as compared to 50-MHz velocities for large flow angles. They typically had the situation with HF/VHF data overlapped at far HF ranges (in the present study for such a situation we also had smaller HF velocities).

To explain the VHF and HF velocity relationship, one has to keep in mind several circumstances. First of all, the range profile of the VHF velocity is determined by two major factors, variation due to aspect angle and a change in the background electric field with latitude (range). The as-

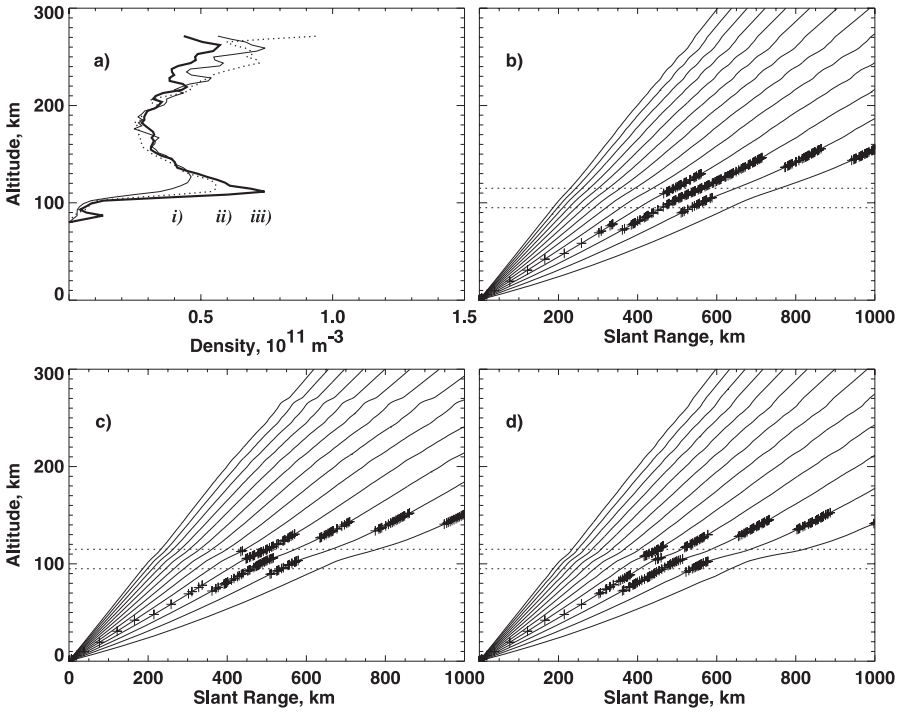

Fig. 13. (a) Three electron density profiles measured by EISCAT at 14:50 UT (case (i)), 14:10 UT (case (ii)) and 14:30 UT (case (iii)) and **(b)**−**(d)** possible ray paths for 12.4-MHz radar waves at Hankasalmi, Finland. The ray paths are shown in elevation angle step of 2° for the elevations between 6° and 30°. Crosses indicate ranges where the aspect angle of the ray with the Earth's magnetic flux line is less than 1°. Horizontal dotted lines indicate the electrojet irregularity layer between 95 and 115 km.

pect angles are worse at shorter ranges, leading to a VHF velocity decrease, as explained above. One might expect an additional decrease in the VHF velocity due to, perhaps, the lower heights (than usual 110 km) of the VHF echoes at shorter ranges since the aspect angles are better at the bottom of the electrojet layer. At lower heights, collisional effects might decrease the irregularity phase velocity (Uspensky et al., 1994). We should note that the EISCAT measurements showed low electron densities below ~ 105 km, minimizing the chance for this effect to happen. In addition to the above plasma physics' decrease in the VHF velocity at short ranges, one might expect that the electric field also decreases equatorward of the auroral oval (Rich and Hairston, 1994).

For the HF velocity, the range profiles are more difficult to explain. As a starting point, one can follow Uspensky et al. (1994), who assumed that the observed HF velocity can be described by the linear theory formula and assumed that the received HF signal comes from a wide range of heights. Then the range profiles should have a maximum of the power matched with the maximum of the velocity. These maxima correspond to that part of the ionosphere where the aspect angles are around zero, roughly at the center of the electrojet. At distances shorter and farther away from this range of the power and velocity maximum, the HF velocity decreases, in particular rather quickly at shorter ranges, due to the aspect angle effect.

In this way, one can explain the relative variations of the HF velocity with range, but there is still a problem with the absolute values of expected velocities (unless special electron density profiles are assumed). At the range of the velocity maximum, Uspensky et al.'s (1994) model predicts only a small difference between the HF velocity and the convection velocity ($V_{\rm HF} \cong 0.8\,V_{\rm E}$). In observations, the differences were probably stronger; we concluded that the VHF velocity was greatly reduced by more than a factor of 2 with respect to the convection velocity at the range of the HF velocity maximum ($V_{\rm VHF} < 0.5\,V_{\rm E}$ at the EISCAT spot). Since the VHF velocity is about the same as the HF velocity at the maximum, one has to conclude that the HF velocity magnitudes were more than 3 times smaller than the convection velocity ($V_{\rm HF} < 0.3\,V_{\rm E}$). This implies that the simple approach, proposed by Uspensky et al. (1994), does not work in our case. We suggest that perhaps the linear theory formula does describe properly the aspect variation (trend) of the HF velocity, but not the absolute values. If this statement is correct, then one can explain the larger (smaller) HF (VHF) velocities at short (far) distances as a result of the aspect angle effect, similar to Uspensky et al. (1994). We should note that the smaller HF E-region velocity as compared to the $\boldsymbol{E} \times \boldsymbol{B}$ velocity was explained in the past by using the idea that the irregularity velocity can be modified by the background plasma gradients (e.g. Hanuise et al., 1991). This explanation is not applicable to our observations, since the coherent radar measurements were carried out outside the FB instability cone.

One might think that neutral winds greatly modified the observed HF and VHF velocities, as Kohl et al. (1992) stipulated. The neutral wind might affect both the HF and VHF velocity. Since at the range of HF echo power maxima the aspect angles of VHF echoes are worse, the neutral wind is expected to affect VHF velocities the strongest, since the neutral wind effect in velocity is significant for irregularities propagating/observed at large aspect angles (Makarevitch et al., 2001). For the period 14:00–15:00 UT in our event the

predominantly westward neutral wind of ~ 80 m/s was observed at the electrojet heights of ~ 106 km (C. Meek, personal communication, MF radar observations at Tromsø). Such a wind would provide an additional component (less than 80 m/s) to the VHF velocity on top of the component provided by the electric field-related particle motions (consider the ion contribution to the irregularity phase velocity according to the linear theory formula; Fejer and Kelley, 1980). This would mean that the observed VHF velocities actually corresponded to a smaller V_E (some Doppler shift is due to neutral wind) and consequently, the difference between the observed HF velocities and V_E is not as large as we just concluded.

Another effect potentially contributing to low HF velocities (as compared to V_E) can be the HF echo contamination by low-height scatter. Danskin et al. (2002) performed ray-tracing analysis for some intervals of the 12 February 1999 event and showed that echo reception from the D-region heights is very likely for the period under discussion, their Fig. 7d. We made a more elaborate ray-tracing analysis in this study. In Fig. 13 we show three electron density profiles measured by EISCAT during the period of E/E comparison and the corresponding ray-tracing diagrams. Here two neighboring ray paths differ in 2° of elevation angle with an overall range of angles between 6° and 30°. For ray-tracing calculations, the EISCAT electron densities were scaled down by a factor of 2 for the following reasons. First, for smaller densities, there is a reasonable agreement between the prediction of the E-region echo ranges and the measurements. Second, the Sodankyla ionosonde, observing at similar magnetic latitude as the location of the echoes, showed densities that were about 2 times smaller. Also, an electron density decrease equatorward of the auroral oval can be expected (e.g. Rino et al., 1983).

If HF echoes were indeed strongly affected by scatter from the bottom of the electrojet layer, or even from the D-region, then one might expect two effects. First, there could be some wind contribution to the observed HF velocity. For the event under study, a southeast wind of up to 50 m/s was observed below ~ 100 km over Tromsø. If the electric field were oriented northward (as it was at near Tromsø), then one would expect the neutral wind contribution to the irregularity phase velocity to be of an opposite polarity than the electric field contribution. Thus, the neutral wind can decrease the HF velocity by perhaps ~ 20–30 m/s. This is an additional factor in the decreasing of HF velocities (with respect to V_E). The other effect is the possibility of decameter irregularities formation due to wind-related plasma instabilities (Kagan and Kelley, 1998; 2000). For such instabilities the irregularity phase velocity is not so strongly controlled by the electric and magnetic fields as in the case of pure FB or GD waves. The thermal instability considered by Dimant and Sudan (1995, 1997) might be of importance as well. A further check on the feasibility of both of the above explanations requires detailed information on the electric field magnitude and orientation, plus the wind distribution in the D-region /bottom E-region, neither of which are available.

Finally, we would like to mention that the seemingly easy task of VHF-HF comparison is quite difficult in practice. In searching for appropriate events, we noticed that very often only either CUTLASS or STARE echoes were observed, but not both. This effect is evident even for the data presented in this study. In Fig. 4c one can see that the strongest HF echoes occurred around 13:00 UT. At this time, the VHF echoes almost completely disappeared, Fig. 4a, probably in response to a general decrease in both the ambient electric field and the electron density, but perhaps other factors were involved. Chaturvedi et al. (1994), by analyzing the excitation of the GD irregularities in the electrically coupled E- and F-layers, concluded that there might be an interrelation between the excitation processes in the E- and F-regions, when one of the layers is strongly inhomogeneous. In our case, the E-layer was undergoing rapid changes (around 13:00 UT), which might have boosted the GD instability in the F-layer. Such processes might affect the phase velocity of the irregularities, but more data are needed to discuss these issues.

7 Conclusions

New results obtained in this study are as follows:

- The STARE Finland double-pulse velocities, for observations outside of the FB instability cone, can be 2–3 times smaller than the $\boldsymbol{E} \times \boldsymbol{B}$ convection along a radar beam for significant periods of time (1–2 h) and in a broad band of ranges (300–400 km in slant range). The effect is more pronounced for short slant ranges of $<$700–800 km, where the aspect angles of measurements are the worst possible. Strongly reduced double-pulse velocities outside of the FB instability cone were also observed by the STARE Norway radar at the range of the EISCAT CP-1 spot.

- In spite of significantly decreased double-pulsed STARE velocities, as compared to the convection magnitude (measured by EISCAT), application of the standard STARE merging procedure gives a reasonable estimate of the convection azimuth, the property known for the periods when the velocity outside of the FB instability cone is a cosine component of the convection (e.g. Reinleitner and Nielsen, 1985). This perhaps means that the phase velocity of meter-scale irregularities outside of the FB cone is proportional to the cosine component of the convection velocity, as predicted by the fluid linear theory of the FB and GD instabilities. The effect of a strong velocity decrease (as compared to the convection component) can be explained by the non-zero aspect angles of the STARE radar measurements, especially for the Finland radar measurements at short ranges of observations.

- The above results mean that STARE double-pulse convection estimates, using not only standard merging technique but also the IAA approach (Nielsen and Schlegel,

1985), can deviate significantly from the true convection, especially for predictions at the equatorial and western edges of the STARE field-of-view. The expected deterioration of the STARE convection estimates still needs verification by independent measurements.

– Comparison of the CUTLASS (HF) and STARE (VHF) velocities for observations in the E-region shows that the HF velocity can be smaller, equal, or larger than the VHF velocity, depending on the range of the comparison. At short (far) ranges, the HF (VHF) velocity magnitude is typically larger than the VHF (HF) velocity magnitude. For intermediate ranges, where the HF power and velocity magnitude are at maxima, the HF and VHF velocities are comparable. The observed velocity differences can be explained by different amounts of radio-wave refraction at VHF and HF, so that at short (far) ranges the aspect angles of STARE (CUTLASS) observations are worse. In such an explanation it is assumed that STARE echoes originate from irregularities produced by the FB and GD plasma instabilities in a broad range of electrojet heights. Contrary to the pure electrojet nature of the VHF echoes, the HF echoes are perhaps strongly contaminated by scatter from heights of less than 100 km, where the neutral wind might be contributing to the irregularity excitation and HF velocity modification. We also consider the possibility of decameter irregularity generation by purely neutral wind related instabilities (that should give irregularities with low phase velocities), though no data are presented to substantiate this suggestion.

Acknowledgements. CUTLASS Finland radar is supported by PPARC, the Swedish Institute for Space Physics, Uppsala, and the Finnish Meteorological Institute. The STARE system is operated jointly by the Max Plank Institute for Aeronomie, Germany, and the Finnish Meteorological Institute, Finland, in cooperation with SINTEF, University of Trondheim, Norway. EISCAT is an international facility supported by Finland, France, Germany, Japan, Norway, Sweden and the UK. Data of the Sodankyla ionosonde are acknowledged. A. V. K. acknowledges the Solar-Terrestrial Environment Laboratory of Nagoya University for funding during his stay in Japan. The work was also supported by Academy of Finland to M.V.U. The authors are grateful to K. Schlegel and E. Nielsen for discussions.

The Editor in Chief thanks two referees for their help in evaluating this paper.

References

André, R., Hanuise, C., Villain, J.-P., and Cerisier, J.-C.: HF radars: Multifrequency study of refraction effects and localization of scattering, Radio Sci., 32, 153–168, 1996.

Chaturvedi, P. K., Keskinen, M. J., Ossakow, S. L., and Fedder, J. A.: Effects of field line mapping on the gradient-drift instability in the coupled E- and F-region high-latitude ionosphere, Radio Sci., 29, 317–335, 1994.

Coffey, H.: Geomagnetic and solar data, J. Geophys. Res., 104, 22,819–22,820, 1999.

Danskin, D. W., Koustov A. V., Ogawa, T., Nozawa, S., Nishitani, N., Milan, S., Lester, M., and André, D.: On the factors controlling the occurrence of F-region coherent echoes, Ann. Geophysicae, 2002, accepted.

Davies, J. A., Lester, M., Milan, S. E., and Yeoman, T. K.: A comparison of velocity measurements from the CUTLASS Finland radar and the EISCAT UHF system, Ann. Geophysicae, 17, 892–902, 1999.

Dimant, Ya. S. and Sudan, R. N.: Kinetic theory of the Farley-Buneman instability in the E-region of the ionosphere, J. Geophys. Res., 100, 14 605–14 623, 1995.

Dimant, Ya. S. and Sudan, R. N.: Physical nature of a new cross-field current-driven instability in the lower ionosphere, J. Geophys. Res., 102, 2551–2563, 1997.

Fejer, B. G. and Kelley, M. C.: Ionospheric irregularities, Rev. Geophys., 18, 401–454, 1980.

Gurevitch, A. V., Borisov, N. D., and Zybin, K. P.: Ionospheric turbulence induced in the lower part of the E-region by the turbulence of the neutral atmosphere, J. Geophys. Res., 102, 379–388, 1997.

Greenwald, R. A., Weiss, W., Nielsen, E., and Thomson, N. R.: STARE: A new radar auroral backscatter experiment in Northern Scandinavia, Radio Sci., 13, 1021–1029, 1978.

Greenwald, R. A., Baker, K. B., Dudeney, J. R., et al.: DARN/SuperDARN: A global view of the dynamics of high-latitude convection, Space Sci. Rev., 71, 763–796, 1995.

Haldoupis, C. and Schlegel, K.: Direct comparison of 1-m irregularity phase velocity and ion-acoustic speeds in the auroral E-region ionosphere, J. Geophys. Res., 95, 18 989 -19 000, 1990.

Hanuise, C., Villain, J.-P., Cerisier, J. C., Senior, C., Ruohoniemi, J. M., Greenwald, R. A., and Baker, K. B.: Statistical study of high-latitude E-region Doppler spectra obtained with SHERPA HF radar, Ann. Geophysicae, 9, 273–285, 1991.

Kagan, L. M. and Kelley, M. C.: A wind-driven gradient drift mechanism for mid-latitude E-region ionospheric irregularities, Geophys. Res. Lett., 25, 4141–4144, 1998.

Kagan, L. M. and Kelley, M. C.: A thermal mechanism for generation of small-scale irregularities in the ionospheric E-region, J. Geophys. Res., 105, 5291–5303, 2000.

Kohl, H., Nielsen, E., Rinnert, K., and Schlegel, K.: EISCAT results during the ROSE campaign and comparison with STARE measurements, J. Atmos. Terr. Phys., 1992, 54, 733–739, 1992.

Koustov, A. V., Igarashi, K., André, D., Ohtaka, K., Sato, N., Yamagishi, H. and Yukimatu, A. S.: Observations of 50- and 12-MHz auroral coherent echoes at the Antarctic Syowa station, J. Geophys. Res., 106, 12 875–12 887, 2001.

Kustov, A. V. and Haldoupis, C.: Irregularity drift velocity estimates in radar auroral backscatter, J. Atmos. Terr. Phys., 54, 415–423, 1992.

Kustov, A. V., Koehler, J. A., Sofko, G. J., Danskin, D. W., and Schiffler, A.: Relationship of the SAPPHIRE-North merged velocity and the plasma convection velocity derived from simultaneous SuperDARN radar measurements, J. Geophys. Res., 102, 2495–2501, 1997.

Kustov, A. V., Uspensky, M. V., Kangas, J., Huuskonen, A., and Nielsen, E.: Effect of the altitude profile of auroral scattering on electric field measurements in the STARE experiment, Geom. Aeronomie, 30, 384–388, 1990.

Kustov, A. V., Uspensky, M. V., Sofko, G. J., Koehler, J. A., and Mu, J.: Aspect angle dependence of the radar aurora Doppler velocity, J. Geophys. Res., 99, 2131–2144, 1994.

Makarevitch, R. A., Ogawa, T., Igarashi, K., Koustov, A. V., Sato,

N., Ohtaka, K., Yamagishi, H., and Yukimatu, A. S.: On the power-velocity relationship for 12- and 50-MHz auroral coherent echoes, J. Geophys. Res., 106, 15 455–15 469, 2001.

Nielsen, E.: Aspect angle dependence of mean Doppler velocities of 1-m auroral plasma waves, J. Geophys. Res., 91, 10 173–10 177, 1986.

Nielsen, E.: Coherent radar technique, World Ionosphere/Thermosphere Study, WITS Handbook, Vol 2, (Ed) Liu, C. H., ICSU/SCOSTEP, U. of Illinois, 1989.

Nielsen, E. and Schlegel, K.: Coherent radar Doppler measurements and their relationship to the ionospheric electron drift velocity, J. Geophys. Res., 90, 3498–3504, 1985.

Nielsen, E., del Pozo, C. F., and Williams, P. J. S.: VHF coherent radar signals from the E-region ionosphere and the relationship to electron drift velocity and ion-acoustic velocity, J. Geophys. Res., 107, (A1), 10.1029/2001JA900111, 2002.

Ogawa, T., Balsley, B. B., Ecklund, W. L., Carter, D. A., and Johnston, P. E.: Auroral radar observations at Siple Station, Antarctica, J. Atmos. Terr. Phys., 44, 529–537, 1982.

Providakes, J. F., Farley, D. T., Fejer, B. G., Sahr, J., Swartz, W. E., Haggstrom, I., Hedberg, A., and Nordling, J. A.: Observations of auroral E-region plasma waves and electron heating with EISCAT and a VHF RADAR interferometer, J. Atmos. Terr. Phys., 50, 339–356, 1988.

Reinleitner, L. A. and Nielsen, E.: Self-consistent analysis of electron drift velocity measurements with the STARE/SABRE system, J. Geophys. Res., 90, 8477–8486, 1985.

Rich, F. J. and Hairston, M.: Large-scale convection patterns observed by DMSP, J. Geophys. Res., 99, 3827–3844, 1994.

Rino, C. L., Livingston, R. C., Tsunoda, R. T., Robinson, R. M., Vickrey, J. F., Senior, C., Cousins, M. D., Owen, J., and Klobuchar, J. A.: Recent studies of structure and morphology of auroral zone F-region irregularities, Radio Sci., 18, 1167–1180, 1983

Robinson, T. R.: Simulation of convection flow estimation errors in VHF bistatic auroral radar systems, Ann. Geophysicae, 11, 1033–1050, 1993.

Sahr, J. D. and Fejer, B. G.: Auroral electrojet plasma irregularity theory and experiment: A critical review of present understanding and future directions, J. Geophys. Res., 101, 26 893–26 909, 1996.

Schlegel, K.: Interpretation of auroral radar experiments using a kinetic theory of the two-stream instability, Radio Sci., 18, 108–118, 1983.

Schlegel, K.: Coherent backscatter from ionospheric E-region plasma irregularities, J. Atmos. Terr. Phys., 58, 933–941, 1996.

Schlegel, K. and Thomas, E. C.: Reply, J. Geophys. Res., 93, 5987, 1988.

Starkov, G. V., Oksman, J., Uspensky, M. V., and Kustov, A. V.: On the dependence of radar aurora amplitude on ionospheric electron density, J. Geophysics, 52, 49–52, 1983.

Tsunoda, R. T.: High latitude irregularities: A review and synthesis, Rev. Geophys., 26, 719–760, 1988.

Uspensky, M. V., Kustov, A. V., Sofko, G. J., Koehler, J. A., Villain, J.-P., Hanuise, C., Ruohoniemi, J. M., and Williams, P. J. S.: Ionospheric refraction effects in slant range profiles of auroral HF coherent echoes, Radio Sci., 29, 503–517, 1994.

Williams, P. J. S., Jones, B., Kustov, A. V., and Uspensky, M. V.: The relationship between E-region electron density and the power of auroral coherent echoes at 45 MHz, Radio Sci., 34, 449–457, 1999.